PHYSICAL REVIEW B **92**, 220403(R) (2015)

Critical damping constant of a spin torque oscillator with a perpendicularly magnetized free layer and an in-plane magnetized reference layer

Hiroko Arai,[1,2] Rie Matsumoto,[2] Shinji Yuasa,[2] and Hiroshi Imamura[2,*]

[1]*JST PRESTO, Kawaguchi, Saitama 332-0012, Japan*

[2]*National Institute of Advanced Industrial Science and Technology (AIST), Spintronics Research Center, Tsukuba, Ibaraki 305-8568, Japan*

(Received 1 October 2015; revised manuscript received 17 November 2015; published 7 December 2015)

We theoretically analyzed the effects of damping on spin torque induced oscillation in a spin torque oscillator with a perpendicularly magnetized free layer and an in-plane magnetized reference layer. It was found that there exists an unexpectedly small critical damping constant, above which no steady-state oscillation can be excited by spin torque. It was also found that the critical damping constant is almost independent of the anisotropy constants but increases with the spin polarization of the injected current.

DOI: 10.1103/PhysRevB.92.220403 PACS number(s): 85.75.−d, 75.30.Gw, 75.78.−n

A spin torque oscillator (STO) is a nanosized microwave oscillator utilizing the spin torque (ST) induced magnetization dynamics and magnetoresistance effect [1–13]. It has been attracting a great deal of attention from both scientific and application points of view. The STO with a perpendicularly magnetized free layer (p-FL) and an in-plane magnetized reference layer (i-RL) is one of the promising candidates for practical applications because of its high emission power and narrow linewidth [11–13]. The ST induced oscillation in this type of STO was first demonstrated by Rippard *et al.* in magnetic nanocontact devices [11]. In their experiments, the output power was only in the order of 1 nW because the STO was based on the giant magnetoresistance effect with a small magnetoresistance ratio [14,15]. Recently, Kubota *et al.* fabricated a MgO-based STO nanopillar and successfully enhanced the output power up to the order of 1 μW [12] owing to the high magnetoresistance ratio of the MgO-based magnetic tunnel junctions [16–19].

In this type of STO, it has been assumed that the trajectory of the steady-state oscillation is a circle of latitude, i.e., equienergy circle on the Bloch sphere [11,12]. This assumption enables us to treat the dynamics of the polar and azimuthal angles of the magnetization separately and therefore makes analysis much simpler. This assumption is justified in the limit of the small damping constant α. However, even for a small α (0.01), the effects of deviation of the trajectory from the equienergy circle on the oscillation properties such as critical current and oscillation frequency were clearly observed [13]. Therefore, it is important to study how such oscillation properties depend on α. It is also important to investigate a critical value of the damping constant for ST induced oscillation, if it exists.

In this Rapid Communication, the effects of α on ST induced oscillation are analyzed based on the macrospin model. We find that there exists a critical value of the damping constant α_c above which no steady-state oscillation can be excited by ST. The value of α_c is much smaller than unity, which is the critical value for magnetic field induced switching. The dependence of α_c on the anisotropy constant and spin polarization are also discussed.

*h-imamura@aist.go.jp

Figure 1(a) shows a schematic illustration of a circular-shaped pillar type STO and the coordinate system. The x and y axes are taken to be the in-plane directions, while the z axis is taken to be the out-of-plane direction. The STO is assumed to be so small that the magnetization dynamics can be described by the macrospin model, which is justified for a disk with a diameter of less than a few tens of nanometers. The unit vectors $\boldsymbol{m}$ and $\boldsymbol{p}$ represent the magnetization directions of the FL and the RL, respectively. The magnetization of the RL is assumed to be fixed along the positive x direction by strong antiferromagnetic interlayer exchange coupling with a bottom ferromagnetic layer (pinned layer—not shown in the figure). The ST induced magnetization dynamics in the RL [20] is neglected for simplicity. In the absence of the current, $\boldsymbol{m}$ is aligned along the z axis by uniaxial anisotropy. The positive current is defined such that electrons flow from the FL to the RL.

The FL has first- and second-order uniaxial anisotropy, and the magnetic energy is expressed as $E = K_1 \sin^2\theta + K_2 \sin^4\theta + \frac{1}{2}\mu_0 M_s^2 \cos^2\theta$, where θ is the polar angle of $\boldsymbol{m} = (\sin\theta\cos\phi, \sin\theta\sin\phi, \cos\theta)$, μ_0 is the magnetic permeability of vacuum, M_s is the saturation magnetization, and K_1 and K_2 are the first- and second-order uniaxial anisotropy constants, respectively. The last term of E represents the demagnetization energy denoted as E_d. We assume that the FL is so thin that E_d is expressed only in terms of m_z.

The dynamics of $\boldsymbol{m}$ is obtained by solving the following Landau-Lifshitz-Gilbert (LLG) equation with the Slonczewski ST term [21,22],

$$\frac{d\boldsymbol{m}}{d\tau} = -\boldsymbol{m}\times\boldsymbol{h}_{\rm eff} + \frac{\beta}{1+P^2\boldsymbol{m}\cdot\boldsymbol{p}}\boldsymbol{m}\times(\boldsymbol{m}\times\boldsymbol{p}) + \alpha\boldsymbol{m}\times\frac{d\boldsymbol{m}}{d\tau}, \quad (1)$$

where $\tau = \gamma M_s t$ and $\boldsymbol{h}_{\rm eff}$ are dimensionless time and effective field, respectively. Here, γ is the gyromagnetic ratio, and P is the polarization factor of a spin current. The effective field acting on $\boldsymbol{m}$ is given by

$$\boldsymbol{h}_{\rm eff} = -\frac{1}{\mu_0 M_s^2}\frac{\partial E}{\partial \boldsymbol{m}} = \left(\kappa_1^{\rm eff} + 2\kappa_2\sin^2\theta\right)\cos\theta\,\boldsymbol{e}_z, \quad (2)$$

where $\kappa_1^{\rm eff} = \kappa_1 - 1$, $\kappa_{1,2} = K_{1,2}/E_d$, and $\boldsymbol{e}_z$ is the unit vector pointing in the positive z direction. The coefficient of the ST

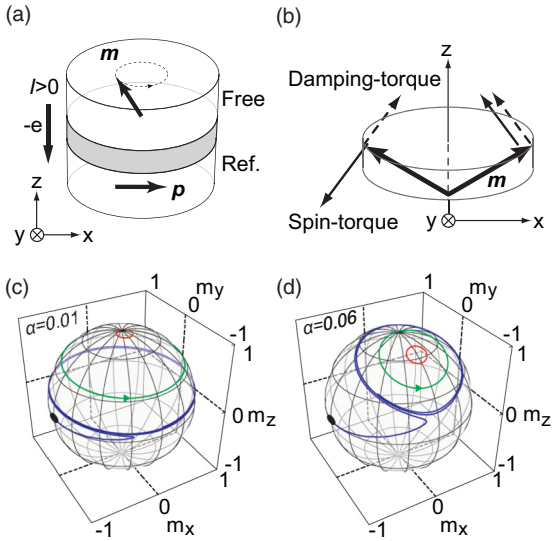

FIG. 1. (Color online) (a) Schematic illustration of a spin torque oscillator with a perpendicularly magnetized free layer (p-FL) and an in-plane magnetized reference layer (i-RL). Positive current is defined such that electrons flow from the FL to the RL. The unit vectors $\boldsymbol{m}$ and $\boldsymbol{p}$ represent the magnetization directions of the FL and the RL, respectively. (b) Directions of spin torque (solid arrow) and damping torque (dashed arrow) acting on $\boldsymbol{m}$. (c) Typical trajectories for $\alpha = 0.01$. From inner to outer, $\beta/\alpha = 3.24$ (red), 5.0 (green), and 5.4 (blue), respectively. (d) Typical trajectories for $\alpha = 0.06$. From inner to outer, $\beta/\alpha = 3.2$ (red), 3.29 (green), and 3.3 (blue), respectively. For (c) and (d), the following parameters are used: $\kappa_1^{\rm eff} = 0.4$, $\kappa_2 = 0.2$, and $P = 0.5$. The fixed point is indicated by the solid circle.

term in Eq. (1) is defined as $\beta = \hbar I P/(2|e|\mu_0 M_s^2 V)$, where $\hbar$ is the Dirac constant, I is the current, e is the electron charge, and V is a volume of the FL. Hereafter we will refer to β/α as the normalized current. The anisotropy constants are assumed to satisfy the condition

$$\frac{\kappa_2}{\kappa_1^{\rm eff}} > \frac{1}{2P^4}\left[\frac{2}{\sqrt{1-P^4}} - (2+P^4)\right], \tag{3}$$

which is necessary for a ST induced oscillation in the absence of an external magnetic field [13].

The mechanism for how the steady-state oscillation is induced by ST is as follows. The ST and damping torque acting on $\boldsymbol{m}$ are schematically illustrated in Fig. 1(b) by the thin solid and dashed arrows, respectively. Since the direction of the ST is given by $\boldsymbol{m} \times (\boldsymbol{m} \times \boldsymbol{p})$, the ST acts as an extra damping for $m_x > 0$ while it acts as a negative damping for $m_x < 0$. If one applies a direct current, which is large enough to balance the energy gain owing to the ST with the energy loss due to the damping torque over one oscillation period, the steady-state oscillation of $\boldsymbol{m}$ is maintained. It should be noted that the trajectory is raised up to the north pole for $m_x > 0$ while it is lowered down to the equator for $m_x < 0$. Since the rotation direction of the steady-state oscillation is given by the vector $\boldsymbol{e}_z \times \boldsymbol{m}$, as indicated by the arrow in Figs. 1(c) and 1(d), the rotation axis of the steady-state oscillation tilts toward the negative y direction.

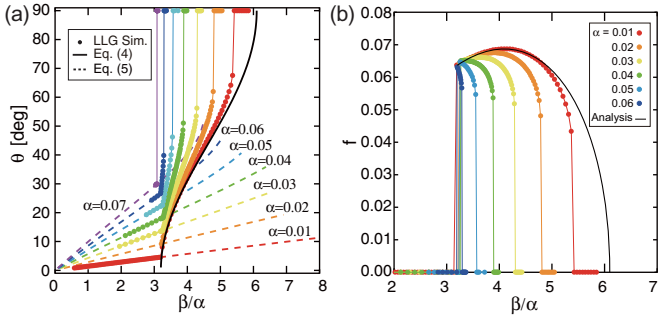

FIG. 2. (Color online) (a) Polar angle of the steady-state oscillation as a function of β/α. The solid black curve corresponds to Eq. (4). The dashed lines represent Eq. (5) for different values of the damping constant α. The solid circles denote the results of numerical simulations for each α with the same color as the dashed lines. The parameters are the same as those in Fig. 1(c). (b) Dimensionless oscillation frequency obtained from numerical simulations as a function of β/α for different values of α. The solid black line represents an analytical result derived in Ref. [13].

Figure 1(c) shows the typical trajectories of the ST induced dynamics for $\alpha = 0.01$. The other parameters are as follows: $\kappa_1^{\rm eff} = 0.4$, $\kappa_2 = 0.2$, and $P = 0.5$. From the inner to the outer, the normalized current is $\beta/\alpha = 3.24$ (red), 5.0 (green), and 5.4 (blue), respectively. The rotation axis of the steady-state oscillation (red and green) slightly but clearly tilts toward the negative y direction. For $\beta/\alpha = 5.4$, the trajectory (blue) ends at the fixed point of $m_x = -1$, which is indicated by the solid black circle. A further increase of β cannot extricate $\boldsymbol{m}$ from the fixed point. The trajectory of ST induced dynamics is sensitive to the increase of α, as shown in Fig. 1(d), where $\alpha = 0.06$ is assumed. Other parameters are the same as those in Fig. 1(c). From the inner to the outer, the normalized current is $\beta/\alpha = 3.2$ (red), 3.29 (green), and 3.3 (blue), respectively. Although the value of $\alpha = 0.06$ is still much smaller than unity, the rotation axis of the steady-state oscillation tilts largely compared with the results of $\alpha = 0.01$.

In Fig. 2(a), the polar angle of steady-state oscillation is plotted as a function of β/α. The solid black curve shows the analytical result [13] given by

$$\frac{\beta}{\alpha} = -P^2 g(\theta)\sin^2\theta\left(1 - \frac{1}{\sqrt{1-P^4\sin^2\theta}}\right)^{-1}, \tag{4}$$

where $g(\theta) = \kappa_1^{\rm eff} + 2\kappa_2\sin^2\theta$. Equation (4) was derived by assuming that the trajectory of the steady-state oscillation is a circle of latitude. The dashed lines represent the polar angle of the fixed point obtained by solving $d\boldsymbol{m}/d\tau = 0$ as

$$\frac{\beta}{\alpha} = \frac{1}{\alpha} g(\theta)\cos\theta\sin\theta. \tag{5}$$

There are two characteristic values of β/α. One defines the threshold current for the ST induced oscillation, which is denoted as $\beta_c^{(1)}/\alpha$. The other, denoted as $\beta_c^{(2)}/\alpha$, defines the critical current above which $\boldsymbol{m}$ stays at a fixed point of $m_x = -1$. Under the assumption that the trajectory of the steady-state oscillation is a circle of latitude, the approximate value of

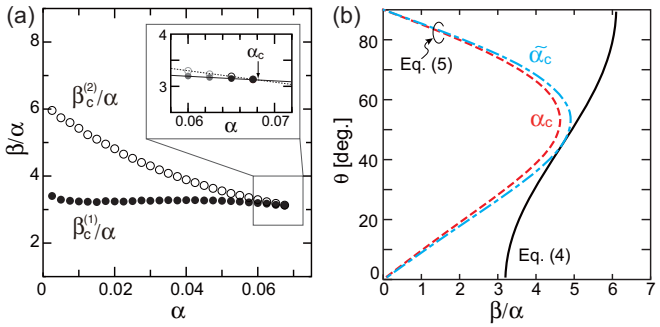

FIG. 3. (Color online) (a) First and second critical currents, $\beta_c^{(1)}/\alpha$ and $\beta_c^{(2)}/\alpha$, are plotted against α. Inset: Linear functions are the fits to $\beta_c^{(1,2)}/\alpha$ at the last two points, $\alpha = 0.0650$ and $\alpha = 0.0675$. The intersecting point of linear fits representing $\alpha_c = 0.0681$ is indicated by the arrow. (b) β/α dependence of the polar angle of steady-state oscillation. The solid curve (black) represents Eq. (4). The dashed red curve represents Eq. (5) for $\alpha = \alpha_c$. The dotted-dashed blue curve, which is tangential to the solid curve, represents Eq. (5) for the approximate value of α_c denoted as $\tilde{\alpha_c}$.

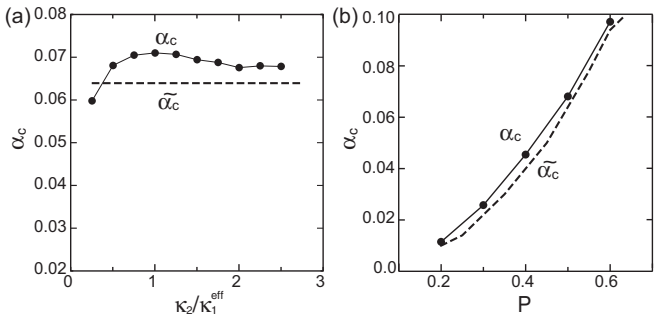

FIG. 4. (a) Critical damping constant α_c (solid circles) and approximate value $\tilde{\alpha_c}$ (dashed line) are plotted as a function of $\kappa_2/\kappa_1^{\rm eff}$. (b) α_c and $\tilde{\alpha_c}$ are plotted as a function of P. Solid circles denote the results obtained by numerical simulations.

$\beta_c^{(1)}/\alpha$ is given by taking the limit of $\theta \to 0$ in Eq. (4) as

$$\frac{\beta_c^{(1)}}{\alpha} \simeq \frac{2\kappa_1^{\rm eff}}{P^2}. \tag{6}$$

The approximate value of the other characteristic value of β/α is also obtained by taking the limit of $\theta \to \pi/2$ in Eq. (4) as

$$\frac{\beta_c^{(2)}}{\alpha} \simeq \frac{1 - P^4 + \sqrt{1 - P^4}}{P^2}\left(\kappa_1^{\rm eff} + 2\kappa_2\right). \tag{7}$$

The solid circles in Fig. 2(a) represent the results obtained by numerically integrating Eq. (1) for each α with the same color as the dashed lines. Parameters other than α are the same as those in Fig. 1(c). In the numerical calculations, the polar angle of the oscillation is obtained from m_z averaged over 1 ns after reaching steady-state oscillation. The deviation of the numerical results from the analytical result indicated by the black curve increases with increasing α. The steady-state oscillation is obtained for $\alpha = 0.01$–0.06, but not for $\alpha \geqslant 0.07$, which implies that there exists a critical value of the damping constant above which no steady-state oscillation can be excited.

The dimensionless oscillation frequencies corresponding to the results shown in Fig. 2(a) are plotted in Fig. 2(b) as functions of β/α. The black curve represents the analytical result derived in Ref. [13]. Since $\beta_c^{(1)}/\alpha$ is almost independent of α, the oscillation frequency at $\beta_c^{(1)}/\alpha$, f_c, is also almost independent of α, as seen in Fig. 2(b). For small α (<0.03), the oscillation frequency takes a maximum value $f_{\rm max}$ at a certain value of β/α other than $\beta_c^{(1)}/\alpha$. For $\alpha \geqslant 0.03$, however, $f_{\rm max}$ is merged into f_c, and the oscillation frequency monotonically decreases with increasing β/α.

Let us focus on the critical damping constant α_c. In Fig. 3(a), numerically obtained values of $\beta_c^{(1)}/\alpha$ and $\beta_c^{(2)}/\alpha$ are plotted as a function of α by the solid and open circles, respectively. Parameters other than α are the same as those in Fig. 1(c). The region of the normalized current providing steady-state oscillation, $\beta_c^{(1)}/\alpha < \beta/\alpha < \beta_c^{(2)}/\alpha$, decreases with increasing α and disappears at a certain critical value of α. A magnified view for the region $0.058 \leqslant \alpha \leqslant 0.072$ is shown in the inset of Fig. 3(a). The solid and dashed lines are respectively the linear fits of $\beta_c^{(1)}/\alpha$ and $\beta_c^{(2)}/\alpha$ of the data points at $\alpha = 0.065$ and 0.0675. The critical value of the damping constant is determined to be $\alpha_c = 0.0681$ by the crossing point of these two lines, as indicated by the down arrow. It should be noted that the obtained value of α_c is much smaller than unity, which is the critical damping constant for field switching.

For practical applications, it is important to obtain the approximate value of the critical damping constant $\tilde{\alpha_c}$ without solving the LLG equation directly. Let us define $\tilde{\alpha_c}$ by the value of α, at which the curves representing Eqs. (4) and (5) are tangential to each other, as shown by the dotted-dashed blue and solid black curves in Fig. 3(b). This crude approximation is based on the finding that the curve representing Eq. (5) for α_c is very close to that for $\tilde{\alpha_c}$, as shown in Fig. 3(b). As will be shown below, this definition of $\tilde{\alpha_c}$ actually gives a value fairly close to α_c. Moreover, it enables us to predict the dependence of α_c on anisotropy constants and spin polarization.

The value of $\tilde{\alpha_c}$ is easily obtained by substituting the value of θ at a tangential point into the equation representing α satisfying both Eqs. (4) and (5) given by

$$\alpha = P^2 \cot\theta \left(\frac{1}{\sqrt{1 - P^4 \sin^2\theta}} - 1 \right). \tag{8}$$

It should be noted that Eq. (8) is independent of the anisotropy constants because both Eqs. (4) and (5) depend in the same way on the anisotropy constants through $g(\theta)$. Therefore, $\tilde{\alpha_c}$ is independent of the anisotropy constants. In Fig. 4(a), we plot α_c and $\tilde{\alpha_c}$ as a function of $\kappa_2/\kappa_1^{\rm eff}$ by the solid circles and the dashed line, respectively. Parameters other than κ_2 are the same as those in Fig. 1(c). One can clearly see that α_c is almost independent of $\kappa_2/\kappa_1^{\rm eff}$ and $\tilde{\alpha_c}$ is actually a good approximation for α_c.

From Eq. (8), on the other hand, one can expect that $\tilde{\alpha_c}$ and therefore α_c will increase with P. In Fig. 4(b), we plot α_c and $\tilde{\alpha_c}$ as a function of P by the solid circles and dashed curve, respectively. Parameters other than P are the same as those in Fig. 1(c). As shown in Fig. 4(b), both α_c and $\tilde{\alpha_c}$ increase with an increase of P, as expected, and $\tilde{\alpha_c}$ is a very good approximation for α_c.

In summary, we analyzed the effects of damping on ST induced oscillations in a STO with a p-FL and i-RL. We found that there is a critical damping constant for the ST induced oscillation, which is much smaller than unity. The critical damping constant was shown to be almost independent of the anisotropy constants but to increase with an increase of the spin polarization. A method to obtain a good approximate value of the critical damping constant without numerically solving the LLG equation was also provided.

We would like to thank Takehiko Yorozu for valuable discussions. This work was partially supported by JST PRESTO, and by JSPS KAKENHI Grant No. 23226001.

[1] S. I. Kiselev, J. C. Sankey, I. N. Krivorotov, N. C. Emley, R. J. Schoelkopf, R. A. Buhrman, and D. C. Ralph, Nature (London) **425**, 380 (2003).

[2] M. D. Stiles and J. Miltat, in *Spin Dynamics in Confined Magnetic Structures III*, edited by B. Hillebrands and A. Thiaville, Topics in Applied Physics No. 101 (Springer, Berlin, 2006), pp. 225–308.

[3] A. M. Deac, A. Fukushima, H. Kubota, H. Maehara, Y. Suzuki, S. Yuasa, Y. Nagamine, K. Tsunekawa, D. D. Djayaprawira, and N. Watanabe, Nat. Phys. **4**, 803 (2008).

[4] G. Bertotti, in *Magnetic Nanostructures in Modern Technology*, edited by B. Azzerboni, G. Asti, L. Pareti, and M. Ghidini (Springer, Berlin, 2008), pp. 37–60.

[5] A. Slavin and V. Tiberkevich, IEEE Trans. Magn. **45**, 1875 (2009).

[6] P. M. Braganca, B. A. Gurney, B. A. Wilson, J. A. Katine, S. Maat, and J. R. Childress, Nanotechnology **21**, 235202 (2010).

[7] K. Kudo, T. Nagasawa, K. Mizushima, H. Suto, and R. Sato, Appl. Phys. Express **3**, 043002 (2010).

[8] H. Maehara, H. Kubota, Y. Suzuki, T. Seki, K. Nishimura, Y. Nagamine, K. Tsunekawa, A. Fukushima, A. M. Deac, K. Ando, and S. Yuasa, Appl. Phys. Express **6**, 113005 (2013).

[9] H. Suto, T. Nagasawa, K. Kudo, K. Mizushima, and R. Sato, Nanotechnology **25**, 245501 (2014).

[10] S. Tamaru, H. Kubota, K. Yakushiji, T. Nozaki, M. Konoto, A. Fukushima, H. Imamura, T. Taniguchi, H. Arai, T. Yamaji, and S. Yuasa, Appl. Phys. Express **7**, 063005 (2014).

[11] W. H. Rippard, A. M. Deac, M. R. Pufall, J. M. Shaw, M. W. Keller, S. E. Russek, G. E. W. Bauer, and C. Serpico, Phys. Rev. B **81**, 014426 (2010).

[12] H. Kubota, K. Yakushiji, A. Fukushima, S. Tamaru, M. Konoto, T. Nozaki, S. Ishibashi, T. Saruya, S. Yuasa, T. Taniguchi, H. Arai, and H. Imamura, Appl. Phys. Express **6**, 103003 (2013).

[13] H. Arai, R. Matsumoto, S. Yuasa, and H. Imamura, Appl. Phys. Express **8**, 083005 (2015).

[14] M. N. Baibich, J. M. Broto, A. Fert, F. Nguyen Van Dau, F. Petroff, P. Etienne, G. Creuzet, A. Friederich, and J. Chazelas, Phys. Rev. Lett. **61**, 2472 (1988).

[15] G. Binasch, P. Grunberg, F. Saurenbach, and W. Zinn, Phys. Rev. B **39**, 4828 (1989).

[16] S. Yuasa, T. Nagahama, A. Fukushima, Y. Suzuki, and K. Ando, Nat. Mater. **3**, 868 (2004).

[17] S. S. P. Parkin, C. Kaiser, A. Panchula, P. M. Rice, B. Hughes, M. Samant, and S.-H. Yang, Nat. Mater. **3**, 862 (2004).

[18] D. D. Djayaprawira, K. Tsunekawa, M. Nagai, H. Maehara, S. Yamagata, N. Watanabe, S. Yuasa, Y. Suzuki, and K. Ando, Appl. Phys. Lett. **86**, 092502 (2005).

[19] S. Yuasa and D. D. Djayaprawira, J. Phys. D: Appl. Phys. **40**, R337 (2007).

[20] R. Matsumoto, H. Kubota, T. Yamaji, H. Arai, S. Yuasa, and H. Imamura, Jpn. J. Appl. Phys. **53**, 123001 (2014).

[21] J. Slonczewski, J. Magn. Magn. Mater. **159**, L1 (1996).

[22] J. C. Slonczewski, Phys. Rev. B **71**, 024411 (2005).